Solar-driven valorization of glycerol towards production of chemicals and hydrogen

Solar-driven valorization of glycerol towards production of chemicals and hydrogen

Valeriia Maslova,[a,b] Andrea Fasolini,[a] Michele Offidani,[a] Stefania Albonetti,[a,*] Francesco Basile[a,c,*]

[a]*Dip. Chimica Industriale "Toso Montanari", Università di Bologna, Viale Risorgimento 4, 40136 Bologna (BO), Italy*

[b]*Université de Lyon, C2P2 (UMR 5265 CNRS, Université de Lyon 1, CPE Lyon), France*

[c]*Consorzio Interuniversitario di Reattività Chimica e Catalisi, CIRCC, via Celso Ulpiani, 27, 70126 Bari (BA), Italy*

***Corresponding authors:** Francesco Basile f.basile@unibo.it ; Stefania Albonetti stefania.albonetti@unibo.it

Keywords: Photocatalytic reforming, Glycerol, TiO_2, Hydrogen production, Biomass valorization

Abstract

Reverse microemulsion-based synthesis was successfully applied to the preparation of nanosized TiO_2 particles in anatase and rutile crystalline phases. The resulted nano-oxides were found to have smaller average crystalline size, higher surface area and narrower band gap than commercial TiO_2 samples, P25 and DT-51. All the TiO_2 materials were used as supports for platinum nanoparticles prepared by incipient wetness impregnation and deposition-precipitation methods. The photo-catalytic activities of these materials were compared in the reaction of glycerol photo-reforming in aqueous media using simulated solar light. The results showed that different crystalline phases of titania have different effects on hydrogen production and selectivity of intermediate products. Anatase was found to be more selective towards glyceraldehyde, while the presence of rutile promoted a more selective reaction towards glycolaldehyde. Rutile also exhibited a higher productivity of hydrogen compared to anatase.

1. Introduction

Increasing energy demand and extensive utilization of fossil sources are considered to be among the reasons of a global increase of energy-related CO_2 emissions [1]. Therefore, introduction of renewable, low-carbon sources nowadays is progressing fast [2], [3].

One of the forward-looking concepts towards sustainability is to utilize solar energy, a renewable, abundant, cheap and carbon-free source of energy, as to drive catalytic process [4],[5]. In particular, the field of heterogeneous photo-catalysis have advanced in the last decades from decomposition of pollutants and water splitting to a more complex reactions such as selective organic synthesis [6],[7],[8],[9],[10] and CO_2 reduction [11],[12]. Recent publications in the field of

heterogeneous photo-catalysis have demonstrated the feasibility of converting oxygenated organic substrates into hydrogen by means of photo-reforming process using semiconducting materials, staring from model compounds [13],[14],[15],[16],[17] to a more complex systems such as plastics [18],[19], lignin [20],[21], and biomass-derived crude glycerol [22],[23].

Recently, thermo-, electro- and photo-catalytic valorization of glycerol, by-product of biodiesel production, has been considered as sustainable way to obtain various high valuable chemicals [24],[25] and hydrogen as energy carrier [26],[27] due to the fast-growing global market of biodiesel and, thus, low price of crude glycerol [28]. In particular, photo-reforming of glycerol have received a substantial attention by many authors in the last decade due to high rates of H_2 production compared to the majority of studied mono- and polyols [29]. Among the catalysts reported for glycerol photo-reforming, TiO_2-based materials have drawn the greatest interest, because they are cheap, non-toxic, abundant and non-critical raw materials [30], having a good thermal and photo-stability. Most of the studied photo-catalysts consist of a noble metal co-catalyst which serves as cathode or electron trap, thus, responsible for H_2 evolution. On the opposite, the surface of semiconductor is considered as anodic site, where the photo-generated hole participates in oxidation of substrate [13],[31],[32]. Interestingly, the majority of these studies report monitoring the rates of hydrogen production, thus focusing only on the reduction reaction. The mechanism of oxidation side is seldom discussed in detail.

This work presents the results on photocatalytic reforming of glycerol in aqueous media using TiO_2 semiconductor supported Pt nanoparticles. Two commercially available and two lab-synthesized titania having different phase compositions were used. As far as synthesis of titania concerns, the microemulsion-mediated method was used. This method have a number of advantages compared to traditional ones: it improves the size distribution and allows controlling the size and morphology of nanoparticles [33],[34],[35]. Moreover, microemulsion technique allows to easily tune TiO_2 composition by varying the synthesis conditions, as it will be demonstrated in this work. Recently, it has been demonstrated that TiO_2 prepared by microemulsion method outperformed the differently synthesized titania in the reaction of glycerol photo-reforming, carried out in similar conditions, thanks to a greater specific surface area, giving access to the increased densities of active sites. [36] Besides, this method provides an improved control over mixed oxide and bimetallic system composition, where the initial ratio of the precursor concentrations in the micelles will correspond to the final composition of the particles obtained after post-treatment [37],[38],[39]. As the crystalline size, specific surface area and polymorph composition of the support are among the parameters that can substantially influence photocatalytic performance [40], [41], [42], [43], [44], the microemulsion technique was selected to obtain anatase and rutile phases to be compared with commercial supports. The effect of different phases of titania and metal co-catalyst on hydrogen production and selectivity of intermediate products in glycerol photo-reforming are assessed taking into account the method of co-catalyst and TiO_2 preparation.

2. Experimental part

2.1. Materials

P25 (TiO_2 P25 Degussa), DT-51 (TiO_2 DT-51 Millennium CrystalACTIV) were used as commercially available references as received; Titanium(IV) butoxide (97%, Sigma Aldrich), Triton X-100 (Alfa Aesar), 1-hexanol (99%, Alfa Aesar), Cyclohexane (99%, Alfa Aesar), Ethanol (99.8%, Sigma Aldrich), HNO_3 (65%, Sigma Aldrich) were used for the synthesis of titania by reverse microemulsion method; $[Pt(NH_3)_4](NO_3)_2$ (99.99%, Alfa Aesar, Premion®), $H_2PtCl_6 \cdot xH_2O$ (Sigma Aldrich) were used for the Pt nanoparticles preparation; glycerol (99.5% Alfa Aesar), glyceraldehyde (90%, Sigma-Aldrich), glycolaldehyde dimer (Sigma-Aldrich), dihydroxyacetone dimer (97%, Sigma-Aldrich) were used for High Performance Liquid Chromatography (HPLC) calibration and as Nuclear Magnetic Resonance (NMR) standards, all without further purification.

2.2. Catalyst preparation

TiO_2 nano-oxides were prepared by reverse microemulsion method following the procedure reported elsewhere [45], modifying the thermal treatment. In brief, the oil phase composed by cyclohexane (dispersant), Triton X-100 (surfactant), and n-hexanol (co-surfactant), was mixed with 5 M aqueous solution of HNO_3, forming a microemulsion system. Another oil phase was prepared adding titania precursor, titanium (IV) butoxide. This solution was added to previously prepared microemulsion under vigorous stirring. The resulting reverse microemulsion system was stirred for 1 h at room temperature, and then heated up to 74°C under reflux and kept at this temperature for 5 h under vigorous stirring. The resulting solid was separated by centrifugation and washed with ethanol 5 times. The obtained paste was dried overnight at 100°C and calcined at 400°C for 3 h with the ramp of 2°C/min. The resulting solid powder of titania in the form of anatase was denominated as TiO_2-m_A.

Titanium dioxide with rutile phase was obtained, following the same procedure, except the stirring was kept for 4 days at room temperature, without further heat-treatment. The obtained precipitate was then separated, washed, dried and calcined as mentioned above. The resulting powder was denominated as TiO_2-m_R.

Platinum metal nanoparticles were deposited by incipient wetness impregnation and deposition-precipitation (DP) of platinum precursor following the reduction step in hydrogen flow. For the impregnation procedure, the solution of $H_2PtCl_6 \cdot x\ H_2O$ was loaded on powders, containing the same pore volume as the volume of the added precursor solution, following cycles of loading and drying in oven at 100°C. Finally, the powder was dried at 120°C overnight, calcined at 350°C for 3h (ramp 10°C/min) in static air and sieved with 60-80 mesh. The Pt NPs were obtained by reduction in H_2/N_2 flow (100 cm^3/min, 10%) at 350°C for 3h (ramp 10°C/min) in static air. The DP synthesis was performed as follow: a 0.001M solution of $[Pt(NH_3)_4](NO_3)_2$ was used at pH 8, adjusted by adding dropwise a 0.1 M NaOH solution. Then, the resulting solution was added dropwise to the titanium

dioxide suspension under vigorous stirring at room temperature with a dropwise addition of 0.1 M NaOH to maintain pH 8. Once the entire platinum solution was transferred, temperature was increased to 65°C, and the obtained suspension was stirred for 2 h. The solid was then separated by centrifugation, washed several times with water, dried at 110°C overnight and calcined at 350°C for 3 h with a rate of 10°C/min in static air and sieved with 60-80 mesh. The Pt NPs were obtained by reduction with H_2/He flow (100 cm^3/min, 5%) at 350°C for 3h (ramp 10°C/min). According to the type of synthesis, resulting catalysts were denoted as Pt/TiO_2-m_A, Pt/TiO_2-m_A_DP; Pt/TiO_2-m_R, Pt/TiO_2-m_R_DP; Pt/P25, Pt/P25_DP; Pt/DT-51, Pt/DT-51_DP. All the platinum-containing solids were loaded on titania in 1.5wt.% of Pt. **Table 1** reports all prepared samples.

2.3. Catalyst characterization

The prepared materials were characterized in terms of their specific surface area, phase composition and light absorption properties, using nitrogen physisorption at the temperature of liquid nitrogen, X-ray diffraction (XRD), Raman and diffuse reflectance UV-vis spectroscopy (DRS).

Catalyst surface area was measured by a N_2 physisorption apparatus (Sorpty 1750 CE instruments) and single-point BET analysis methods, in which samples were pre-treated under a vacuum at 125°C.

Powder X-ray diffraction analyses of all the samples were carried out at room temperature with a Bragg/Brentano diffractometer (X'pertPro PANalytical) equipped with a fast X'Celerator detector, using a Cu anode as the X-ray source (Kα, λ=1.5418 Å). Diffractograms were recorded in the range of 10-80°2θ with a step of 0.05°2θ. Particle size determination was done by Scherrer equation over the 100% peak. The rutile-to-anatase ratio for all the samples was determined according to the method described by Ding et al. [46].

Raman spectra were recorded at ambient temperature with 514 nm Ar^+ laser excitation by Renshaw RM1000 spectrometer equipped with Leica DMLM microscope and CCD camera. Power output was 6.25 mW and grating 1200 lines/mm.

Diffuse reflectance UV-vis spectroscopy analyses were carried out in a Perkin Elmer Lambda 19 instrument equipped with integrating sphere in the range 280-800 nm.

Temperature programmed desorption (TPD) of ammonia and carbon dioxide analyses were carried out on a Micromeritics Autochem II instrument equipped with TCD detector. In temperature programmed NH_3 desorption analysis, the sample was first pre-treated at 400°C for 45 min (ramp 10°C/min) in He atmosphere (30 cm^3/min). The sample was flushed for 1 h at 100°C with a mixture of 10% NH_3 in He (30 cm^3/min), then it was purged for 1 h with helium at the same temperature. Finally, desorption measurements were carried out up to 700°C with a ramp of 10°C/min with isotherm of 30 min. In temperature programmed CO_2 desorption analysis, the sample was first pre-treated at 500°C for 2 h (ramp 10°C/min) in He atmosphere (30 cm^3/min). Saturation of the sample with carbon dioxide (10% in He) was carried out at 60°C for 1 h (30 cm^3/min). Desorption measurements were performed in He for 30 min up to 900°C (ramp 10°C/min) for 20 min.

Transmission electron microscopy (TEM) analysis of platinum containing samples were done at IMM_CNR, Bologna, Italy. The analyses were carried out using TEM/STEM FEI TECNAI F20 instrument, equipped with a high-angle annular dark field (HAADF) detector at 200 keV. The corresponding samples were suspended in ethanol and treated in ultrasonic bath for 15 minutes. The suspension was deposited on a "quantifoil carbon film" Cu grid for TEM analysis, then dried at 100°C.

2.4. Photocatalytic test and analytical methods

The photo-reforming of glycerol has been carried out in a sealed top-irradiated glass photo-reactor (**Scheme S1**). Prior the reaction, 7% by volume (1M), aqueous solution of glycerol with 0.5 g/L of catalyst were stirred for 20 min in the dark, while purging continuously N_2. The amount of catalyst was optimized following H. Kisch [47] and presented **in Figure S1**. The sealed reactor of 4.6 cm diameter was irradiated for 6 h using the solar simulator that consists of 300 W Xe-lamp (irradiance of 100 mW/cm^2 was regularly measured prior each test by radiometer HD2102.2 DELTA OHM equipped with two probes of 315-400 nm and 400-1050 nm). Samples were collected at the end of the reaction. After reaction, the samples were qualitatively analyzed by Electrospray Ionization Mass-spectrometry (ESI-MS) and Nuclear Magnetic Resonance (NMR) techniques for identification of the products. Waters micromass ZQ 4000 instrument with quadrupole mass analyzer was used to perform ESI-MS analysis. The aqueous product solution was diluted in methanol and injected without further derivatization. Positive ions conditions were 3.53 kV for the probe and 10 V for the cone, while for negative ions the probe voltage was 2.54 kV and 40 V for the cone with a 0.02 cm^3/min flux. 600 MHz ^{1}H NMR analysis was performed using Varian Inova (600 MHz for 1H) equipped with an indirect triple resonance probe. The data treatment was done using a presaturation sequence (PRESAT, with power=4dB and presaturation delay 2s), while analyzing aqueous solutions (the residual H_2O signal δ 4.79 ppm). After the reaction, the liquid phase was filtered, diluted 100 times (from 1 M to 0.01 M) or used without dilution (in case of 0.05 M), and analyzed in an Agilent HPLC over Rezex ROA Organic Acid column (0.0025M H_2SO_4 eluent, oven temperature 30°C and 0.6 cm^3/min flux) with DAD and RID detectors. Aqueous solutions of commercial standards were used to calibrate the products by external method. Hydrogen was analyzed in off-line Agilent Technologies GC equipped with CP Molesieve 5A UM 25m x 0.53mm x 50µm column and TCD detector. The calibration was done using constant volume (1 cm^3) of gas-tight syringe with different molar fractions of H_2/N_2. The calibration was done injecting different volumes of the commercial mixture of gases with constant molar fraction.

The study of the effect of the reaction time during 10 min, 1 h, 2 h, 3 h and 5 h proceeded with 0.05 M aqueous glycerol solution, keeping the amount of catalyst loading 0.5 g/L. In this set of experiments with the more diluted starting concentration, the conversion of glycerol (*X*%), yield (*Y*%) and selectivity (*S*%) of the products were calculated using the following equations:

$$X\% = \frac{n(glycerol)_{in},mol - n(glycerol)_{fin},mol}{n(glycerol)_{in},mol} \times 100\% \quad \textbf{(Eq. 1)}$$

$$S\% = \frac{n(product),mol \cdot SF}{n(glycerol)_{in},mol - n(glycerol)_{fin},mol} \times 100\% \quad \textbf{(Eq. 2)}$$

While in the experiments with 7% by volume (1M) aqueous solution of glycerol the selectivity of products was calculated as:

$$S\%' = \frac{n(product),mol \cdot SF}{\sum n(product),mol \cdot SF} \times 100\% \quad \textbf{(Eq. 3)}$$

where SF is the stoichiometry factor, which is equal to 1 for glyceraldehyde and dihydroxyacetone, 2/3 for glycolaldehyde, and 1/4 for H_2, n is moles of corresponding product.

3. Results and discussions

3.1. Catalyst characterization

Figure S2 shows the diffractograms of all the used TiO_2 powders. The content of different crystal structures has been estimated for all the materials using the procedure reported by Ding et al. [46]. Commercial TiO_2 P25 consists of 80% anatase and 20% rutile, which is consistent with other works [48]. From XRD data provided in **Figure S2** the crystallite size of anatase in P25 crystals was found 23 nm with respect to anatase (101) reflection. Another commercial TiO_2 (DT-51) nanocrystals consist of 100% anatase with particles diameter of 20 nm. XRD analysis of TiO_2 anatase synthetised by microemulsion (TiO_2-m_A) demonstrate that the main phase is represented by anatase (92%) with a small amount of rutile (8%). From XRD patterns, the crystallite size of TiO_2-m_A calcined at 400°C was determined to be 8 nm, which confirms that the microemulsion technique permitted to obtain small crystallites, indeed. Rutile, in turn, has been considered as the thermodynamically stable above 35 nm at all temperatures and atmospheric pressure [45]. Nevertheless, as one can see from the **Figure S2** and **Table 1**, microemulsion method allows synthesizing rutile with 11 nm crystallites (sample TiO_2-m_R). It is worth noting that the microemulsion synthesis allowed to obtain both, anatase-rich and a pure rutile phase, by just changing the hydrolysis time, highlighting the versatility of this synthetic method.

Table 1. Data obtained from DRS, XRD, N_2 physisorption and TEM measurements.

Catalyst	d_{XRD}[a] (nm)	S_{BET} (m^2/g)	E_g[c] (eV)	d_{TEM} (nm)
TiO_2-m_A	8	130	3.08	-
TiO_2-m_R	11[b]	50	3.02	-
DT-51	20	80	3.26	-
P25	23	49	3.10	-
Pt/TiO_2-m_A_DP	7	128	3.11	0.9
Pt/TiO_2-m_A	8	121	3.11	1.9
Pt/TiO_2-m_R_DP	12	40	2.94	1.5
Pt/TiO_2-m_R	11	50	2.92	1.2
Pt/DT-51_DP	21	62	3.28	0.8
Pt/DT-51	21	57	3.27	2.5
Pt/P25_DP	24	40	3.12	1.0
Pt/P25	23	50	3.10	2.2

[a] Crystalline size of TiO_2 determined from anatase (101) reflection

[b] Particle size determined for rutile (110) reflection by the Scherrer formula

[c] Energy bandgap estimated from KM spectra.

XRD patterns of Pt-containing materials prepared by the incipient wetness impregnation and deposition-precipitation methods with reduction in hydrogen are shown in **Figure S3**. The XRD patterns of Pt-containing materials resemble the data obtained for pristine supports. Thus, the deposition of Pt NPs and treatment of Pt-decorated materials do not affect the crystalline size of TiO_2 as well as the phase composition, keeping anatase as major phase with reflections (101), (004), (200), (105) and (211) at 25.33, 37.82, 48.08, 53.93 and 55.12 2°θ, respectively. The crystalline size was calculated by Scherrer formula using the anatase (101) reflection. The values of crystalline size of prepared materials are shown in **Table 1**. No Pt phase was detected due to the small amount and crystallite size of Pt in the sample.

The phase composition was also confirmed by RAMAN spectroscopy. On **Figure S4** one can see a clear presence of anatase phase in P25, DT-51 and TiO_2-m_A, showing the bands with the corresponding assignments at 143 cm^{-1} (E_g), 197 cm^{-1} (Eg), 397 cm^{-1} (B_{1g}), 516 cm^{-1} (B_{1g}), and 638 cm^{-1} (E_g). While the bands of rutile phase in TiO_2-m_R could be observed at 143, 445 and 610 cm^{-1} with B_{1g}, E_g and A_{1g} symmetry species, respectively. The band at 210 cm^{-1} and a weak broad shoulder at approximately 707 cm^{-1} have been attributed to second-order or two-phonon RAMAN scattering [49],[50],[51].

Specific surface area was determined, and the results are shown in **Table 1** for bare titania. The obtained results indicated that the procedure used for microemulsion-synthesized titania preparation permitted to obtain a photocatalyst with a higher surface area and smaller crystallite size with respect to the commercial powders. **Table 1** shows that P25, TiO_2-m_A, TiO_2-m_R retain their

surface areas even after Pt deposition. On contrast, the surface area of DT-51 notably decreased after deposition of Pt nanoparticles. It is known that anatase normally undergoes a drastic transition to rutile at temperatures starting from 500°C, resulting in shrinking of surface area with the particle size decrease. In a recent study it has been shown that the anatase can retain its phase composition even at 500°C, however a slight growth of particles was observed with a concurrent decrease in surface area [36]. Thus, the minor decrease in specific surface area of DT-51 after Pt deposition may be due to the specific porosity of this commercial sample, than can be partially blocked by the metal deposition.

Diffuse Reflectance Spectroscopy was used to evaluate absorbing capability of solids. Reflectance spectra on **Figure S5** indicate that absorption of TiO_2-m-based powders and P25 is slightly enhanced in the visible region with respect to the commercial DT-51. This behavior could be mainly due to the presence of a small amount of rutile in the lab-synthesized titania and P25, as highlighted from the XRD patterns reported in **Figure S2.** Indeed, the absorption edge for TiO_2-m_R is notably shifted towards visible range compared to other photocatalysts. This is in agreement with literature, since it is known that energy bandgap of rutile is around 3.0 eV, while anatase is characterized by an energy bandgap of around 3.3 eV [52]. To note, however, the band gap can be red shifted by 0.25 eV for oxygen deficient TiO_2 as was reported by T. Das and co-workers [53].

The results in **Table S1** shows that the values of energy bandgap of the different types of titanium dioxide slightly differ depending the method used. [54] Nevertheless, all the samples absorb in the UV range of solar spectrum, and the bandgap calculated using Reflectance, KM or Tauc plot (**Figure S5-S7**) are generally following the same trend, and it decreases in the order: DT-51 > P25 > TiO_2-m_A > TiO_2-m_R. Therefore, it is possible to conclude that all the three methods could be valid for determination and comparison of band gap of powdered materials.

Regarding KM spectra of Pt-decorated samples, **Figure S8** shows a more pronounced increase of absorption intensity throughout visible and NIR region for Pt/TiO_2-m_A_DP compared to pristine supports (**Figure S6**), which could be ascribed to the presence of PtO_x on the surface of semiconductor as was reported in the literature [16],[55],[56]. On the other hand, such increase was explained by a large absorption cross section of noble metal nanoparticles (Au, Pt, Ag) that generate intra- and interband transitions via 6sp and 5d band, producing hot electrons, which are then injected into conduction band of semiconductor occurring at the metal-semiconductor interface. As a result, noble metal nanoparticles facilitate absorption and transfer of visible part of solar energy to semiconductor [16],[57],[58]. From the obtained KM spectra, energy bandgap of the samples were determined and collected in **Table 1**.

TEM micrographs and size distribution of Pt-decorated samples are shown in **Figure S9.** Between two methods, in case of anatase-rich samples, the deposition-precipitation gives access to smaller and homogenously distributed Pt NPs than classical impregnation, although for both methods big platinum clusters (> 2 nm) could be observed. Different situation can be observed for rutile-based samples. TEM images show that incipient wetness impregnation resulted in smaller

platinum clusters than deposition-precipitation with narrower distribution, although clusters of 10 nm were observed in TEM micrographs (**Figure S10, A**). On the other hand, for Pt/TiO_2-m_DP sample, large aggregates of 35 nm can be observed (**Figure S10, B**). The average particle size of Pt is shown in **Table 1**.

3.2. Photocatalytic tests

Photocatalytic glycerol reforming tests were carried out on both bare supports and Pt-TiO_2 catalysts using simulated solar light with the aim to maximize the H_2 productivity compared to literature reports and to study the effect of different titania on liquid phase products, among which, glyceraldehyde, glycolaldehyde, dihydroxyacetone, hydroxyacetone are normally the primary products of this reaction [32],[59],[60]. In **Figure 1**, the tests with only bare supports have revealed a better rate of hydrogen evolution for the material with the greatest fraction of rutile, TiO_2-m_R. The activity trend did not change if normalized to unit area of the semiconductor (**Figure S11**), emphasizing that specific surface area is not the main intrinsic property of the catalyst affecting hydrogen production rates.

Elevated rates of hydrogen production from glucose photo-reforming on rutile-based photo-catalysts were also reported by the groups of M. Bellardita [61] and R. Chong [62]. Nevertheless, in the work of W. Chen and co-workers [44] P25 demonstrated superior activity followed by pure anatase $\approx$ brookite and finally, rutile, towards H_2 in different alcohol-water mixtures due to the anatase-rutile heterojunction, which decreases the rate of electron-hole recombination. However, the morphological and surface area differences between powdered photocatalysts must be taken into account for complete comparison, as well as differences in light distribution for suspended powders, i.e. scattering and absorption. Many theoretical and experimental works conducting the study of scattering and absorption coefficients with the aim to solve radiative transport equation have been reported up to date [63],[64],[65]. Nevertheless, it is beyond the focus of this work.

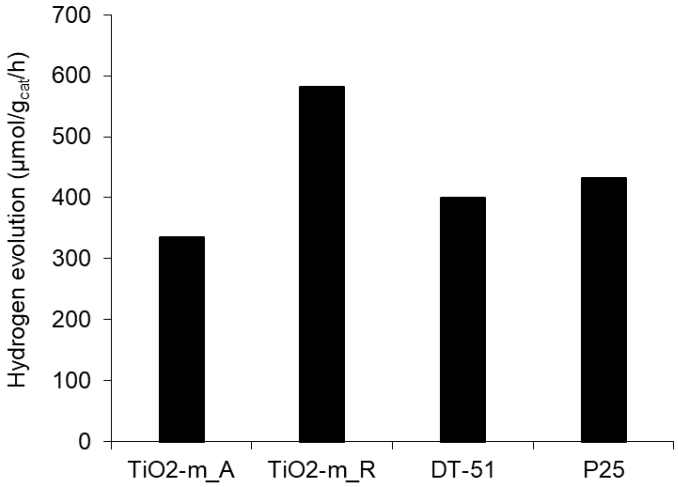

Figure 1. Hydrogen rate evolution for the different types of titania in 7 vol.% aqueous glycerol solution.

Introduction of a metal nanoparticle such as Pt on the surface of TiO_2 significantly enhances the rate of hydrogen production for all the types of TiO_2 as could be seen from **Figure 2**. This enhancement has been previously explained by experiments based on photoluminescence spectroscopy and was associated to the migration of photo-excited electrons from the conduction band of TiO_2 onto the supported metal nanoparticles, and therefore, the decrease of rate in electron-hole recombination phenomena [14],[44],[66]. The use of Pt nanoparticles permitted formation of detectable amount of liquid phase products such as glyceraldehyde and glycolaldehyde, which were the main compounds observed in these conditions. Glycolaldehyde is a well-known high-value compound used as an intermediate for the preparation of other valuable products [67],[68],[69]. For instance, it could be applied as a food browning agent. It is also used as an intermediate for ethylene glycol or ethanolamine synthesis, cross-linking agent for amino-containing materials.

No activity was observed, when the reactions were undergone in the dark or when only the visible light (>420 nm) was used. Except hydrogen and CO_2, among the gas phase products some traces of CO and CH_4 were detected, indicating that the reduction processes may occur, although the electrons do not participate directly in reduction products generation.

Comparing the two methods of Pt NPs preparation, one can see that the catalysts synthesized by deposition-precipitation exhibit higher rates of hydrogen production, but also higher rates of liquid phase products compared to the impregnation method thanks to the well-dispersed small Pt NPs with a high surface area as could be seen in TEM images (**Figure S9**). The advantage of deposition-precipitation synthesis yielding small metal nanoparticles with narrow particle size distribution, regardless the metal loading, was also pointed out in the literature [70],[71]. The exception in this correlation is Pt/TiO_2-m_R with smaller Pt NPs than Pt/TiO_2-m_R_DP, which revealed greater rates of hydrogen production compared to Pt/TiO_2-m_R_DP sample (**Figure 2**), further confirming the positive effect of well-dispersed and small nanoparticles on photo-reforming process. Superior activity of smaller Pt NPs can have two-fold explanation. Firstly, smaller particles

owing its high surface area could effectively participate as cathode, reducing H^+ to H_2. Secondly, the role of co-catalyst in photo-catalysis has been widely investigated [44],[66],[15],[72], elucidating the reason of suppressed electron-hole recombination by the fact that Pt NPs create a rectifying Schottky contact on the surface of TiO_2, thus trapping the electrons photo-excited into the conduction band of TiO_2. Meanwhile the holes, remained in the valence band, efficiently participates in oxidation of organic substrates.

Figure 2 shows that the deposition of Pt NPs changed the activity of rutile-rich titania, TiO_2-m_R. In the shown set of experiments, P25-based materials outperformed the other types of titania supports in hydrogen production. This can be explained by the presence of big aggregations of Pt NPs found for TiO_2-m_R (**Figure S9**, **S10**) that could decrease the dispersion of metal responsible for hydrogen evolution.

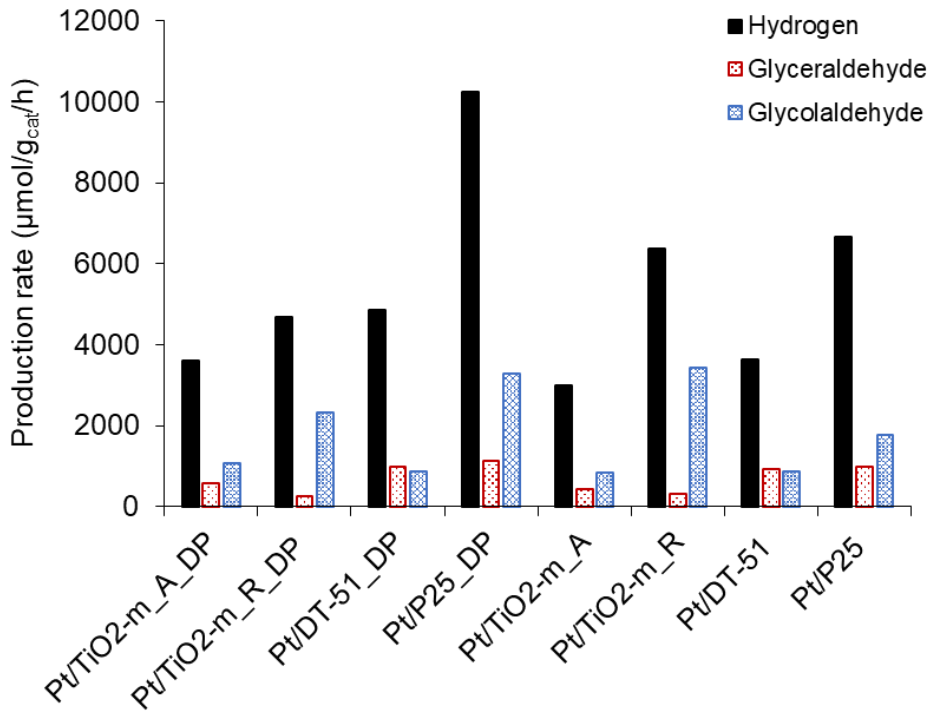

Figure 2. The rate of hydrogen production and the liquid phase products for Pt-supported samples in 7 vol.% aqueous glycerol solution.

Further comparison of the results shown in **Figure 2** demonstrates that P25, TiO_2-m_A and TiO_2-m_R based catalysts exhibit higher production rates of glycolaldehyde, while DT-51 based ones showed slightly greater productivity to glyceraldehyde than glycolaldehyde. This is in agreement with the calculated values of selectivity using these supports, shown in **Table 2**.

Table 2. Selectivity of glyceraldehyde and glycolaldehyde with Pt-supported catalysts on different types of titania using deposition-precipitation (DP) method.

Photo-catalyst	**DT-51_DP**	**TiO_2-m_A_DP**	**P25_DP**	**TiO_2-m_R_DP**
S (glyceraldehyde), %	63	45	34	14
S (glycolaldehyde), %	37	55	66	86

To elucidate whether the differences in mechanism of liquid phase products may originate from different surface acidity and basicity of the supports, the TPD analyses were carried out. The results of temperature-programmed desorption of ammonia analysis for all the titania supports are presented in **Figure 3**. The desorption curves are centered in the range of 150-650°C showing for all the supports a presence of acid sites of different strength. Worth to note, both TiO_2-m_A and TiO_2-m_R have strong acid sites around 600°C, according to classification given in literature [73]. Whereas only TiO_2-m_A and P25 show the presence of a strong acid site above 650°C. The sample TiO_2-m_A is notably characterized by a greater amount of weak and medium acid sites compared to other samples. Such behavior can be explained by a larger surface area of this material [34]. In fact, surface-normalized TPD NH_3 of the supports presented in **Figure 3B** show comparable intensity of TCD signal. Nevertheless, calculated amount of desorbed NH_3 showed greater value for lab-synthesized anatase, TiO_2-m_A, both for mass- and surface area-normalized cases, followed by DT-51, TiO_2-m_R and P25 samples (**Table S2**). The TPD CO_2 curves for all the samples are presented in **Figure 4**. The TPD CO_2 profiles in this case show a convolution of basic sites of different strength for all the supports. In this case a distinguished peak above 700°C can be noticed for DT-51. This behavior could be explained by the decomposition of residues remained from the synthesis of TiO_2 DT-51, namely sulfates and chlorides, also mentioned previously in the literature [74]. While TiO_2-m_A and TiO_2-m_R revealed similar basic sites around 600°C. Surface-normalized TPD CO_2 curves are presented in **Figure 4B**, and does not show a substantial difference as compared to mass-normalized one. The obtained amount of desorbed CO_2 is collected in **Table S2**. The results show that P25 is characterized by a greater amount of basic sites within the studied samples, followed by TiO_2-m_R, TiO_2-A and DT-51.

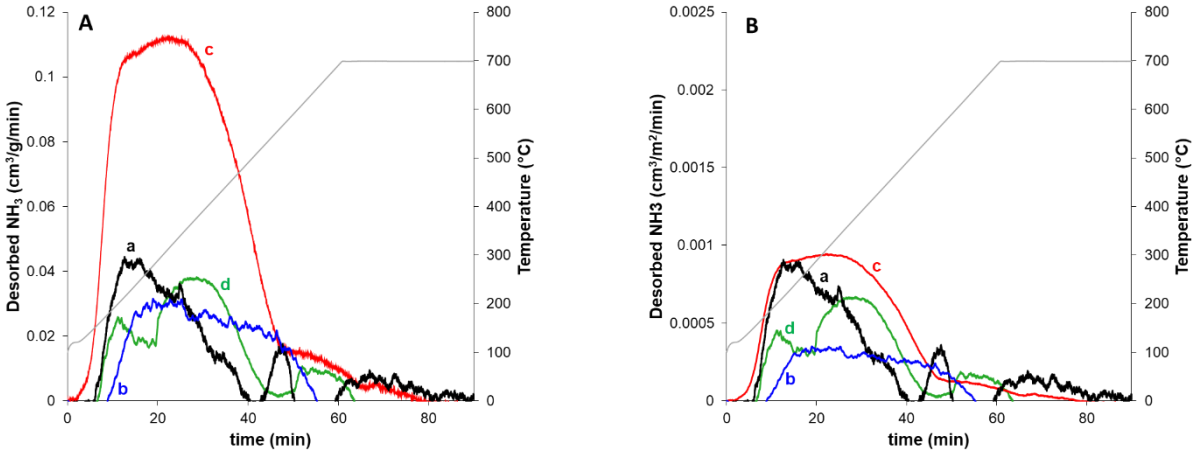

Figure 3. Mass-normalized (A) and surface normalized (B) temperature-programmed desorption of NH_3. Legend: a). P25, b). DT-51, c). TiO_2-m_A, d). TiO_2-m_R.

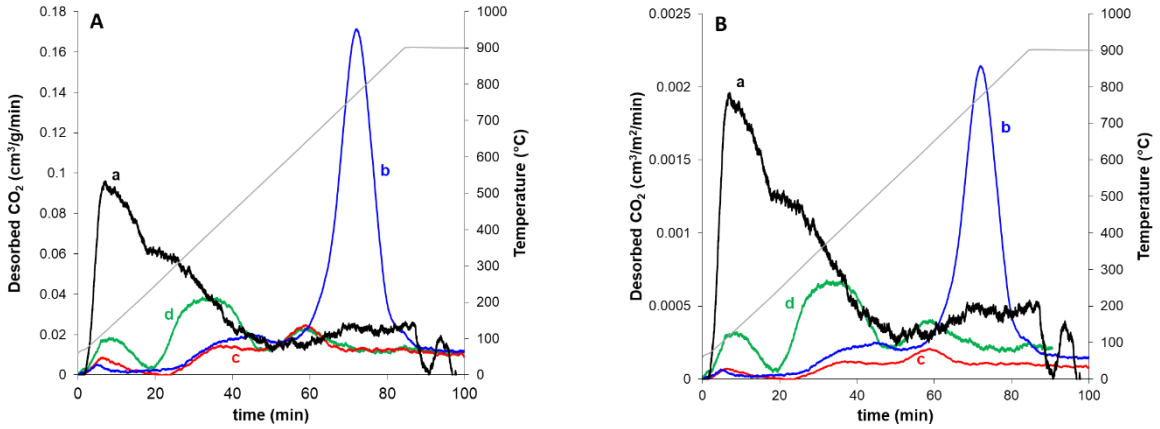

Figure 4. Mass-normalized (A) and surface normalized (B) temperature-programmed desorption of CO_2. Legend: a). P25, b). DT-51, c). TiO_2-m_A, d). TiO_2-m_R.

Comparison of TPD NH_3 and TPD CO_2 did not show evident correlation with results observed on **Figure 2**, suggesting that the photocatalytic reaction unlike the classical catalytic cycles [75],[76] is less sensitive to the acidity of photoactive material. One of the explanations of observed behavior could arise from different mechanism undergone on the surface of different polymorphs of titania (rutile and anatase) upon light absorption. The decrease of glyceraldehyde selectivity and the increase of glycolaldehyde selectivity with the increase of rutile content display preliminary insights towards reaction mechanism for different types of titania.

Taking into account experimental data and literature reported mechanisms over glycerol aqueous phase reforming [77],[26] and photo-reforming [32],[78],[13],[79], it is possible to suggest the scheme of glycerol photo-reforming under study, which is illustrated in **Figure 5**. In this research we have observed formation of glyceraldehyde in the step **1a** as one of the primary products which take place via indirect mechanism described by K. Sanwald and co-worker [32]. In principle, the photo-generated holes are trapped by lattice oxygen sites in TiO_2, abstracting the H-atom from C-H bond with subsequent formation of carbonyl group. One molecule of hydrogen is produced concurrently at a cathodic site. Further oxidation of glyceraldehyde can yield glycolaldehyde and formic acid as indicated in **2a**.

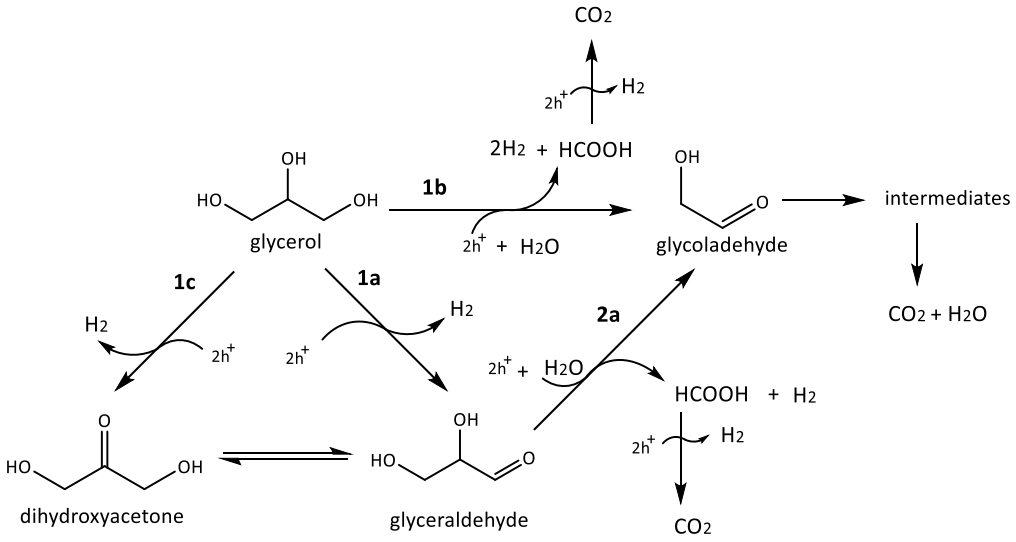

Figure 5. Hypothesized mechanism of glycerol photo-reforming.

This was confirmed with reaction using Pt/DT-51_DP, which has only anatase polymorph. The dependency of selectivity of the products from glycerol conversion, presented in **Figure 6, a,** shows that the primary products of the reaction for DT-51 support are glyceraldehyde and dihydroxyacetone in liquid phase. Then, glycolaldehyde appears as a secondary product with the consumption of both, glyceraldehyde and dihydroxyacetone. However, in the test with microemulsion-synthesized anatase, Pt/TiO_2-m_A_DP (**Figure 6, b**), which has some fraction of rutile, glycolaldehyde can be already observed as a primary product formed directly from glycerol, suggesting the presence of a direct mechanism of C-C cleavage, presumably following step **1b** shown in **Figure 5**. The effect of rutile can be further confirmed in the reaction with Pt/TiO_2-m_R shown in **Figure 6, c.** Analyzing reported in literature mechanism of glycolaldehyde formation on P25-based catalyst, one can suggest direct hole transfer to a chemisorbed glycerol on coordinatively unsaturated Ti(IV)-OH site to generate an alkoxide radical followed by β-C–C-scission [80]. Another suggestion of higher selectivity to glycolaldehyde was given by Chong and co-authors [59]. It is more likely that the peroxy species Ti-O-O-Ti, formed preferentially on rutile {110} in water media, which was confirmed by EPR

and theoretical calculations, are the species responsible for high selectivity to glycolaldehyde. Similar behavior of selective C-C cleavage was observed by the group of M. Bellardita and co-workers [61] on lab-synthesized rutile with and without Pt NPs during the glucose photo-reforming. Authors suggested the presence of peroxo species on rutile being beneficial for milder glucose oxidation than anatase that is known to produce in water highly reactive and surface mobile ·OH radicals leading to over-oxidation of organic molecules. The considerations reported in literature are confirmed in this study where the presence of rutile affects product distribution (**Figure 7**). Glycolaldehyde selectivity increases as rutile content raises, with a concurrent decrease in glyceraldehyde selectivity, showing the importance of this phase in the production of the secondary product.

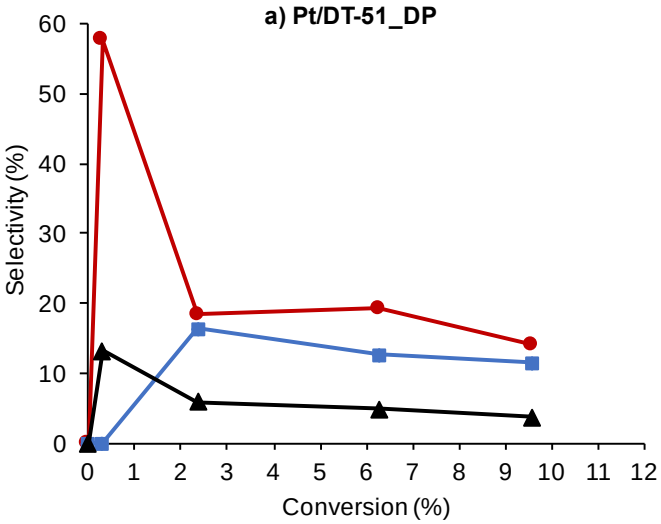

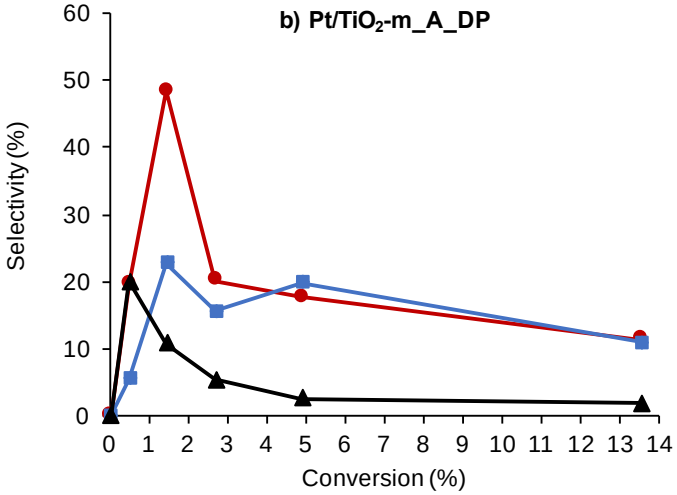

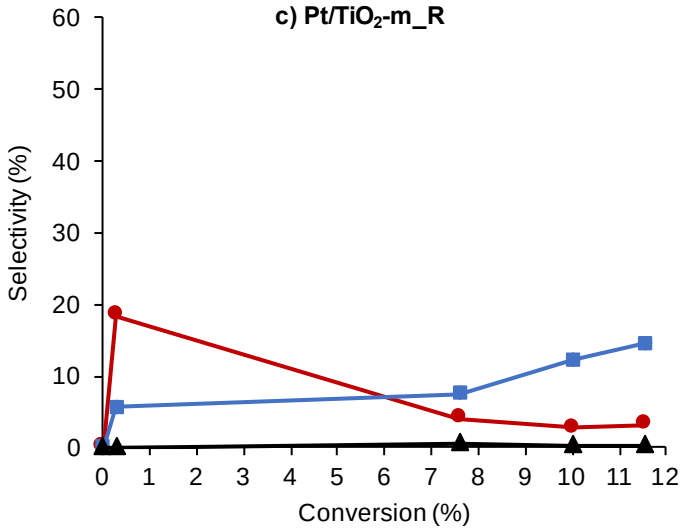

Figure 6. Overall selectivity in the products of interest as a function of the conversion of glycerol for a) Pt/DT-51_DP, and b) Pt/TiO_2-m_A_DP, prepared by deposition-precipitation method, and c) Pt/TiO_2-m_R prepared by wetness incipient impregnation. Conditions: 0.05 M aqueous solution of glycerol; 30°C. Legend: selectivity of glyceraldehyde (●), dihydroxyacetone (▲), glycolaldehyde (■).

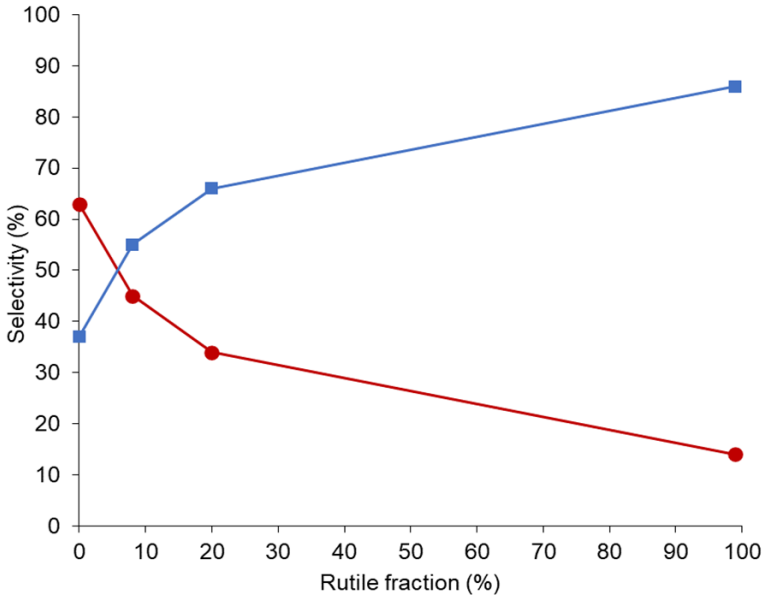

Figure 7. Glyceraldehyde and glycolaldehyde selectivity as function of rutile fraction in the TiO_2 support. Conditions: 0.05 M aqueous solution of glycerol; 30°C. Legend: selectivity of glyceraldehyde (●), dihydroxyacetone (▲), glycolaldehyde (■).

Figure 5 shows also a formation of another C_3-species, dihydroxyacetone, following the step **1c**, via two electron oxidation of secondary carbon atom of glycerol. On the other hand, the formation of dihydroxyacetone could be explained by the fact that in aqueous medium this trios is in fast isomerization equilibrium with glyceraldehyde [81],[82],[83],[84],[85], that in fact take place via an acid-catalyzed hydride shift, via a base-catalyzed mechanism with a proton shift (and intermediate enol), or via a concerted proton-coupled hydride shift in neutral media [86],[87]. Another intermediate such as formic acid is shown in **Figure 5**. Even though formic acid was not detected in liquid phase in this set of experiments, one can assume its formation and fast transformation to carbon dioxide. As a matter of fact, T. Montini and co-workers [79] have shown a complexity of glycerol photo-reforming on Cu/TiO_2 under simulated solar light, meaning the production of multiple intermediates with different rates of formation. A rapid formation and consumption of intermediates often prevents their identification.

This work shows the advantage of microemulsion synthesis in obtaining small crystallites with high specific surface area of anatase-rich and pure rutile TiO_2. The prepared rutile allowed maximizing the rate of hydrogen production from glycerol photo-reforming process compared to commercial benchmark, P25. Moreover, platinized rutile was found to be more active in production of glycolaldehyde via direct C-C cleavage of glycerol.

4. Conclusion

Glycerol photo-reforming toward hydrogen and valuable chemicals production was studied using different polymorphs of titanium dioxide. Within the supports used, lab-synthesized rutile TiO_2-m_R prepared from reverse microemulsion system, demonstrated greater rates of hydrogen production compared to lab-synthesized anatase TiO_2-m_A, and commercially available samples, P25 and DT-51. This activity was changed when Pt metal nanoparticles were deposited on titania, resulting in greater photo-catalytic hydrogen production for P25 support. Among the metal-decorated catalysts tested, Pt nanoparticles prepared by deposition-precipitation showed the most promising results towards hydrogen production, because of the small and homogeneously distributed nanoparticles compared to classical impregnation method. However, rutile-containing samples showed an opposite tendency. The phase composition was found to be affecting the selectivity of liquid phase products. Rutile was more selective to direct C-C cleavage of glycerol to form glycolaldehyde, while anatase was more selective towards glyceraldehyde than to glycolaldehyde. This study opens a possibility to produce chemicals and fuels by photo- or electro-photo-catalytic process, which can be an alternative and efficient way to upgrade biomass feedstock, following current advances in sustainable development.

Acknowledgment

This work was co-funded through a SINCHEM grant. SINCHEM is a Joint Doctorate programme selected under the Erasmus+ Action 1 Programme (FPA 2013-0037). We thank Francesca Ospitali, Department of Industrial Chemistry “Toso Montanari”, for assistance with TEM analysis. We also thank Alessandra Petroli, Department of Industrial Chemistry “Toso Montanari”, Università di Bologna, for assistance with NMR analysis.

Bibliography

[1] https://www.iea.org/reports/global-energy-co2-status-report-2019, (n.d.).

[2] B.C. Marepally, C. Ampelli, C. Genovese, E.A. Quadrelli, S. Perathoner, G. Centi, Production of Solar Fuels Using CO2, in: Horizons Sustain. Ind. Chem. Catal., 1st ed., Elsevier B.V., 2019: pp. 7–30. https://doi.org/10.1016/B978-0-444-64127-4.00001-X.

[3] P. Fabbri, D. Viaggi, F. Cavani, L. Bertin, M. Michetti, E. Carnevale, J. Velasquez Ochoa, G.A. Martinez, M. Degli Esposti, P.K. Fischer, S. Wydra, A. Schwarz, F. Marscheider-Weidemann, Top emerging bio-based products, their properties and industrial applications, 2018.

[4] D.J. Smith, The Past, Present, and Future of Sustainable Chemistry, ChemSusChem. 11 (2018) 5–10. https://doi.org/10.1002/cssc.201702329.

[5] P. Lanzafame, S. Abate, C. Ampelli, C. Genovese, R. Passalacqua, G. Centi, S. Perathoner, Beyond Solar Fuels: Renewable Energy-Driven Chemistry, ChemSusChem. 10 (2017) 4409–4419. https://doi.org/10.1002/cssc.201701507.

[6] A. Lolli, V. Maslova, D. Bonincontro, F. Basile, S. Ortelli, S. Albonetti, Selective oxidation of HMF via catalytic and photocatalytic processes using metal-supported catalysts, Molecules. 23 (2018). https://doi.org/10.3390/molecules23112792.

[7] L. Da Vià, C. Recchi, E.O. Gonzalez-Yañez, T.E. Davies, J.A. Lopez-Sanchez, Visible light selective photocatalytic conversion of glucose by TiO2, Appl. Catal. B Environ. 202 (2017) 281–288. https://doi.org/10.1016/j.apcatb.2016.08.035.

[8] D. Friedmann, A. Hakki, H. Kim, W. Choi, D. Bahnemann, Heterogeneous photocatalytic organic synthesis: State-of-the-art and future perspectives, Green Chem. 18 (2016) 5391–5411. https://doi.org/10.1039/c6gc01582d.

[9] V. Augugliaro, G. Camera-roda, V. Loddo, G. Palmisano, L. Palmisano, J. Soria, S. Yurdakal, Heterogeneous Photocatalysis and Photoelectrocatalysis: From Unselective Abatement of Noxious Species to Selective Production of High-Value Chemicals, J. Phys. Chem. Lett. 6 (2015) 1968–1981. https://doi.org/10.1021/acs.jpclett.5b00294.

[10] Y. Shiraishi, M. Ikeda, D. Tsukamoto, S. Tanaka, T. Hirai, One-pot synthesis of imines from alcohols and amines with TiO2 loading Pt nanoparticles under UV irradiation, Chem. Commun. 47 (2011) 4811–4813. https://doi.org/10.1039/c0cc05615d.

[11] Y. Sohn, W. Huang, F. Taghipour, Recent progress and perspectives in the photocatalytic CO2 reduction of Ti-oxide-based nanomaterials, Appl. Surf. Sci. 396 (2017) 1696–1711.

[12] K. Kočí, K. Matějů, L. Obalová, S. Krejčíková, Z. Lacný, D. Plachá, L. Čapek, A. Hospodková, O. Šolcová, Effect of silver doping on the TiO2 for photocatalytic reduction of CO2, Appl. Catal. B Environ. 96 (2010) 239–244. https://doi.org/10.1016/j.apcatb.2010.02.030.

[13] A. V. Puga, Photocatalytic production of hydrogen from biomass-derived feedstocks, Coord. Chem. Rev. 315 (2016) 1–66. https://doi.org/10.1016/j.ccr.2015.12.009.

[14] K.C. Christoforidis, P. Fornasiero, Photocatalytic Hydrogen Production: A Rift into the Future Energy Supply, ChemCatChem. 9 (2017) 1523–1544. https://doi.org/10.1002/cctc.201601659.

[15] M. Bowker, H. Bahruji, J. Kennedy, W. Jones, G. Hartley, C. Morton, The photocatalytic window: Photo-reforming of organics and water splitting for sustainable hydrogen production, Catal. Letters. 145 (2015) 214–219. https://doi.org/10.1007/s10562-014-1443-x.

[16] F.J. López-Tenllado, J. Hidalgo-Carrillo, V. Montes, A. Marinas, F.J. Urbano, J.M. Marinas, L. Ilieva, T. Tabakova, F. Reid, A comparative study of hydrogen photocatalytic production from glycerol and propan-2-ol on M/TiO2 systems (M=Au, Pt, Pd), Catal. Today. 280 (2017) 58–64. https://doi.org/10.1016/j.cattod.2016.05.009.

[17] M. Yasuda, T. Matsumoto, T. Yamashita, Sacrificial hydrogen production over TiO2-based photocatalysts: Polyols , carboxylic acids , and saccharides, Renew. Sustain. Energy Rev. 81 (2018) 1627–1635.

[18] T. Uekert, H. Kasap, E. Reisner, Photoreforming of Nonrecyclable Plastic Waste over a Carbon Nitride/Nickel Phosphide Catalyst, J. Am. Chem. Soc. 141 (2019) 15201–15210. https://doi.org/10.1021/jacs.9b06872.

[19] T. Uekert, M.F. Kuehnel, D.W. Wakerley, E. Reisner, Plastic waste as a feedstock for solar-driven H2 generation, Energy Environ. Sci. 11 (2018) 2853–2857. https://doi.org/10.1039/c8ee01408f.

[20] H. Kasap, D.S. Achilleos, A. Huang, E. Reisner, Photoreforming of Lignocellulose into H2 Using Nanoengineered Carbon Nitride under Benign Conditions, J. Am. Chem. Soc. 140 (2018) 11604–11607. https://doi.org/10.1021/jacs.8b07853.

[21] C. Li, H. Wang, S.B. Naghadeh, J.Z. Zhang, P. Fang, Visible light driven hydrogen evolution by photocatalytic reforming of lignin and lactic acid using one-dimensional NiS/CdS nanostructures, Appl. Catal. B Environ. 227 (2018) 229–239. https://doi.org/10.1016/j.apcatb.2018.01.038.

[22] N. Lakshmana Reddy, K.K. Cheralathan, V. Durga Kumari, B. Neppolian, S. Muthukonda Venkatakrishnan, Photocatalytic Reforming of Biomass Derived Crude Glycerol in Water: A Sustainable Approach for Improved Hydrogen Generation Using Ni(OH)2 Decorated TiO2 Nanotubes under Solar Light Irradiation, ACS Sustain. Chem. Eng. 6 (2018) 3754–3764. https://doi.org/10.1021/acssuschemeng.7b04118.

[23] P. Ribao, M. Alexandra Esteves, V.R. Fernandes, M.J. Rivero, C.M. Rangel, I. Ortiz, Challenges arising from the use of TiO2/rGO/Pt photocatalysts to produce hydrogen from crude glycerol compared to synthetic glycerol, Int. J. Hydrogen Energy. 44 (2019) 28494–28506. https://doi.org/10.1016/j.ijhydene.2018.09.148.

[24] G. Dodekatos, S. Schünemann, H. Tüysüz, Recent Advances in Thermo-, Photo-, and Electrocatalytic Glycerol Oxidation, ACS Catal. 8 (2018) 6301–6333. https://doi.org/10.1021/acscatal.8b01317.

[25] B. Bharathiraja, I.A.E. Selvakumari, J. Jayamuthunagai, R.P. Kumar, S. Varjani, A. Pandey, E. Gnansounou, Biochemical conversion of biodiesel by-product into malic acid: A way towards sustainability, Sci. Total Environ. 709 (2020) 136206. https://doi.org/10.1016/j.scitotenv.2019.136206.

[26] Y.C. Lin, Catalytic valorization of glycerol to hydrogen and syngas, Int. J. Hydrogen Energy. 38 (2013) 2678–2700. https://doi.org/10.1016/j.ijhydene.2012.12.079.

[27] F. Basile, S. Albonetti, F. Cavani, E. Lombardi, R. Mafessanti, Biosyngas and Derived Products from Gasification and Aqueous Phase Reforming, in: Chem. Fuels from Bio-Based

Build. Blocks, 2016: pp. 79–110.

[28] G. Bagnato, A. Iulianelli, A. Sanna, A. Basile, Glycerol production and transformation: A critical review with particular emphasis on glycerol reforming reaction for producing hydrogen in conventional and membrane reactors, Membranes. 7 (2017) 1–31. https://doi.org/10.3390/membranes7020017.

[29] J. Corredor, M.J. Rivero, C.M. Rangel, F. Gloaguen, I. Ortiz, Comprehensive review and future perspectives on the photocatalytic hydrogen production, J. Chem. Technol. Biotechnol. 94 (2019) 3049–3063. https://doi.org/10.1002/jctb.6123.

[30] M. Gislev, M. Grohol, Report on Critical Raw Materials and the Circular Economy, 2018. https://doi.org/.1037//0033-2909.I26.1.78.

[31] D.I. Kondarides, V.M. Daskalaki, A. Patsoura, X.E. Verykios, Hydrogen production by photo-induced reforming of biomass components and derivatives at ambient conditions, Catal. Letters. 122 (2008) 26–32. https://doi.org/10.1007/s10562-007-9330-3.

[32] K.E. Sanwald, T.F. Berto, W. Eisenreich, O.Y. Gutiérrez, J.A. Lercher, Catalytic routes and oxidation mechanisms in photoreforming of polyols, J. Catal. 344 (2016) 806–816. https://doi.org/10.1016/j.jcat.2016.08.009.

[33] D. Das, A. Shivhare, S. Saha, A.K. Ganguli, Room temperature synthesis of mesoporous TiO2 nanostructures with high photocatalytic efficiency, Mater. Res. Bull. 47 (2012) 3780–3785.

[34] J. Carbajo, A. Bahamonde, M. Faraldos, Photocatalyst performance in wastewater treatment applications : Towards the role of TiO 2 properties, Mol. Catal. 434 (2017) 167–174.

[35] F. Basile, R. Mafessanti, A. Fasolini, G. Fornasari, E. Lombardi, A. Vaccari, Effect of synthetic method on CeZr support and catalytic activity of related Rh catalyst in the oxidative reforming reaction, J. Eur. Ceram. Soc. 39 (2019) 41–52. https://doi.org/10.1016/j.jeurceramsoc.2018.01.047.

[36] V. Maslova, E.A. Quadrelli, P. Gaval, A. Fasolini, S. Albonetti, F. Basile, Highly-dispersed ultrafine Pt nanoparticles on microemulsion-mediated TiO2 for production of hydrogen and valuable chemicals via oxidative photo-dehydrogenation of glycerol, J. Environ. Chem. Eng. 9 (2021) 105070. https://doi.org/10.1016/j.jece.2021.105070.

[37] A. Fasolini, S. Ruggieri, C. Femoni, F. Basile, Highly active catalysts based on the Rh4(CO)12 cluster supported on Ce0.5Zr0.5 and Zr oxides for low-temperature methane steam reforming, Catalysts. 9 (2019) 19. https://doi.org/10.3390/catal9100800.

[38] S. Eriksson, U. Nylén, S. Rojas, M. Boutonnet, Preparation of catalysts from microemulsions and their applications in heterogeneous catalysis, Appl. Catal. A. 265 (2004) 207–219. https://doi.org/10.1016/j.apcata.2004.01.014.

[39] M. Boutonnet, S. Lögdberg, E.E. Svensson, Recent developments in the application of nanoparticles prepared from w / o microemulsions in heterogeneous catalysis, Curr. Opin. Colloid Interface Sci. 13 (2008) 270–286. https://doi.org/10.1016/j.cocis.2007.10.001.

[40] Z. Wu, S. Cao, C. Zhang, L. Piao, Effects of bulk and surface defects on the photocatalytic performance of size- controlled TiO 2 nanoparticles, Nanotechnology. 28 (2017) 1–12.

[41] J. Kou, C. Lu, J. Wang, Y. Chen, Z. Xu, Selectivity Enhancement in Heterogeneous

Photocatalytic Transformations, Chem. Rev. 117 (2017) 1445−1514. https://doi.org/10.1021/acs.chemrev.6b00396.

[42] K. Shimura, H. Yoshida, Heterogeneous photocatalytic hydrogen production from water and biomass derivatives, Energy Environ. Sci. 4 (2011) 2467–2481. https://doi.org/10.1039/c1ee01120k.

[43] G.L. Chiarello, D. Paola, E. Selli, Effect of titanium dioxide crystalline structure on the photocatalytic production of hydrogen, Photochem. Sci. 10 (2011) 335–350. https://doi.org/10.1039/C0PP00158A.

[44] W.-T. Chen, A. Chan, Z.H.N. Al-Azri, A.G. Dosado, M.A. Nadeem, D. Sun-Waterhouse, H. Idriss, G.I.N. Waterhouse, Effect of TiO2 polymorph and alcohol sacrificial agent on the activity of Au / TiO2 photocatalysts for H2 production in alcohol – water mixtures, J. Catal. 329 (2015) 499–513. https://doi.org/10.1016/j.jcat.2015.06.014.

[45] M. Andersson, A. Kiselev, L. Österlund, A.E.C. Palmqvist, Microemulsion-mediated room-temperature synthesis of high-surface-area rutile and its photocatalytic performance, J. Phys. Chem. C. 111 (2007) 6789–6797. https://doi.org/10.1021/jp070284a.

[46] X.Z. Ding, X.H. Liu, Y.Z. He, Grain size dependence of anatase-to-rutile structural transformation in gel-derived nanocrystalline titania powders, J. Mater. Sci. Lett. 15 (1996) 1789–1791. https://doi.org/10.1007/BF00275343.

[47] H. Kisch, Korrespondenz On the Problem of Comparing Rates or Apparent Quantum Yields in Heterogeneous Photocatalysis, Angew. Chem. 122 (2010) 9782–9783. https://doi.org/10.1002/ange.201002653.

[48] Y. Duan, M. Zhang, L. Wang, F. Wang, L. Yang, X. Li, C. Wang, Plasmonic Ag-TiO2-x nanocomposites for the photocatalytic removal of NO under visible light with high selectivity: The role of oxygen vacancies, Appl. Catal. B Environ. 204 (2017) 67–77. https://doi.org/10.1016/j.apcatb.2016.11.023.

[49] S. Challagulla, K. Tarafder, R. Ganesan, S. Roy, Structure sensitive photocatalytic reduction of nitroarenes over TiO 2, Sci. Rep. 7 (2017) 1–11. https://doi.org/10.1038/s41598-017-08599-2.

[50] H.L. Ma, J.Y. Yang, Y. Dai, Y.B. Zhang, B. Lu, G.H. Ma, Raman study of phase transformation of TiO2 rutile single crystal irradiated by infrared femtosecond laser, Appl. Surf. Sci. 253 (2007) 7497–7500.

[51] V. Swamy, Size-dependent modifications of first-order Raman spectra of nanostructured Rutile TiO2, Phys. Rev. B. 77 (2008) 195414(4).

[52] I. Ali, Recent advances in syntheses , properties and applications of TiO 2 nanostructures, RSC Adv. (2018) 30125–30147. https://doi.org/10.1039/c8ra06517a.

[53] T.K. Das, P. Ilaiyaraja, P.S.V. Mocherla, G.M. Bhalerao, C. Sudakar, Influence of surface disorder, oxygen defects and bandgap in TiO2 nanostructures on the photovoltaic properties of dye sensitized solar cells, Sol. Energy Mater. Sol. Cells. 144 (2016) 194–209. https://doi.org/10.1016/j.solmat.2015.08.036.

[54] R. López, R. Gómez, Band-gap energy estimation from diffuse reflectance measurements on sol-gel and commercial TiO 2: A comparative study, J. Sol-Gel Sci. Technol. 61 (2012) 1–7. https://doi.org/10.1007/s10971-011-2582-9.

[55] H. Khan, N. Usen, D.C. Boffito, Spray-dried microporous Pt/TiO2 degrades 4-chlorophenol under UV and visible light, J. Environ. Chem. Eng. 7 (2019) 103267. https://doi.org/10.1016/j.jece.2019.103267.

[56] Y. Hu, X. Song, S. Jiang, C. Wei, Enhanced photocatalytic activity of Pt-doped TiO2 for NOx oxidation both under UV and visible light irradiation: A synergistic effect of lattice Pt4+ and surface PtO, Chem. Eng. J. 274 (2015) 102–112. https://doi.org/10.1016/j.cej.2015.03.135.

[57] Y. Chen, Y. Wang, W. Li, Q. Yang, Q. Hou, L. Wei, L. Liu, F. Huang, M. Ju, Enhancement of photocatalytic performance with the use of noble-metal-decorated TiO2 nanocrystals as highly active catalysts for aerobic oxidation under visible-light irradiation, Appl. Catal. B Environ. 210 (2017) 352–367. https://doi.org/10.1016/j.apcatb.2017.03.077.

[58] Z.H.N. Al-Azri, W.T. Chen, A. Chan, V. Jovic, T. Ina, H. Idriss, G.I.N. Waterhouse, The roles of metal co-catalysts and reaction media in photocatalytic hydrogen production: Performance evaluation of M/TiO2 photocatalysts (M = Pd, Pt, Au) in different alcohol–water mixtures, J. Catal. 329 (2015) 355–367. https://doi.org/10.1016/j.jcat.2015.06.005.

[59] R. Chong, J. Li, X. Zhou, Y. Ma, J. Yang, L. Huang, H. Han, F. Zhang, C. Li, Selective photocatalytic conversion of glycerol to hydroxyacetaldehyde in aqueous solution on facet tuned TiO2-based catalysts, Chem. Commun. 50 (2014) 165–167. https://doi.org/10.1039/c3cc46515b.

[60] P. Panagiotopoulou, E.E. Karamerou, D.I. Kondarides, Kinetics and mechanism of glycerol photo-oxidation and photo-reforming reactions in aqueous TiO 2 and Pt / TiO 2 suspensions, Catal. Today. 209 (2013) 91–98. https://doi.org/10.1016/j.cattod.2012.09.029.

[61] M. Bellardita, E.I. García-López, G. Marcì, L. Palmisano, Photocatalytic formation of H2 and value-added chemicals in aqueous glucose (Pt)-TiO2 suspension, Int. J. Hydrogen Energy. 41 (2016) 5934–5947. https://doi.org/10.1016/j.ijhydene.2016.02.103.

[62] R. Chong, J. Li, Y. Ma, B. Zhang, H. Han, C. Li, Selective conversion of aqueous glucose to value-added sugar aldose on TiO2-based photocatalysts, J. Catal. 314 (2014) 101–108. https://doi.org/10.1016/j.jcat.2014.03.009.

[63] M.I. Cabrera, O.M. Alfano, A.E. Cassano, Absorption and scattering coefficients of titanium dioxide participate suspensions in water, J. Phys. Chem. 100 (1996) 20043–20050. https://doi.org/10.1021/jp962095q.

[64] V. Pareek, S. Chong, M. Tade, A.A. Adesina, Light intensity distribution in heterogenous photocatalytic reactors, Asia-Pac.J.Chem.Eng. 3 (2008) 171–201. https://doi.org/DOI:10.1002/apj.129.

[65] P. Calza, M. Minella, L. Demarchis, F. Sordello, C. Minero, Photocatalytic rate dependence on light absorption properties of different TiO2 specimens, Catal. Today. 340 (2020) 12–18. https://doi.org/10.1016/j.cattod.2018.10.013.

[66] A.G. Dosado, W.T. Chen, A. Chan, D. Sun-Waterhouse, G.I.N. Waterhouse, Novel Au/TiO2 photocatalysts for hydrogen production in alcohol–water mixtures based on hydrogen titanate nanotube precursors, J. Catal. 330 (2015) 238–254. https://doi.org/10.1016/j.jcat.2015.07.014.

[67] P.A. Majerski, J.K. Piskorz, D.S.A.G. Radlein, Production of Glycoldehyde by Hydrous Thermolysis of Sugars. US 7,094,932, n.d.

[68] J. Xu, W. Huang, R. Bai, Y. Queneau, F. Jérôme, Y. Gu, Utilization of bio-based

glycolaldehyde aqueous solution in organic synthesis: Application to the synthesis of 2,3-dihydrofurans, Green Chem. 21 (2019) 2061–2069. https://doi.org/10.1039/c8gc04000a.

[69] K.F. Geoghegan, D.M. Ybarra, R.E. Feeney, Reversible reductive alkylation of amino groups in proteins, Biochemistry. 18 (1979) 5392–5399. https://doi.org/10.1021/bi00591a021.

[70] R. Zanella, S. Giorgio, C.R. Henry, C. Louis, Alternative methods for the preparation of gold nanoparticles supported on TiO2, J. Phys. Chem. B. 106 (2002) 7634–7642. https://doi.org/10.1021/jp0144810.

[71] G.R. Bamwenda, S. Tsubota, T. Nakamura, M. Haruta, Photoassisted hydrogen production from a water-ethanol solution: a comparison of activities of Au-TiO2 and Pt-TiO2, J. Photochem. Photobiol. A Chem. 89 (1995) 177–189.

[72] E. Kowalska, O.O.P. Mahaney, R. Abe, B. Ohtani, Visible-light-induced photocatalysis through surface plasmon excitation of gold on titania surfaces, Phys. Chem. Chem. Phys. 12 (2010) 2344–2355. https://doi.org/10.1039/b917399d.

[73] M. Almohalla, I. Rodríguez-Ramos, A. Guerrero-Ruiz, Comparative study of three heteropolyacids supported on carbon materials as catalysts for ethylene production from bioethanol, Catal. Sci. Technol. 7 (2017) 1892–1901. https://doi.org/10.1039/c7cy00155j.

[74] S. Albonetti, S. Blasioli, R. Bonelli, J.E. Mengou, S. Scirè, F. Trifirò, The role of acidity in the decomposition of 1,2-dichlorobenzene over TiO2-based V2O5/WO3 catalysts, Appl. Catal. A Gen. 341 (2008) 18–25. https://doi.org/10.1016/j.apcata.2007.12.033.

[75] A. Tresatayawed, P. Glinrun, B. Jongsomjit, Ethanol Dehydration over WO3/TiO2 Catalysts Using Titania Derived from Sol-Gel and Solvothermal Methods, Int. J. Chem. Eng. 2019 (2019). https://doi.org/10.1155/2019/4936292.

[76] B. Feng, C. Chen, H. Yang, X. Zhao, L. Hua, Y. Yu, T. Cao, Y. Shi, Z. Hou, Ionic liquid-promoted oxidant-free dehydrogenation of alcohols with water-soluble ruthenium nanoparticles in aqueous phase, Adv. Synth. Catal. 354 (2012) 1559–1565. https://doi.org/10.1002/adsc.201100908.

[77] D.L. King, L. Zhang, G. Xia, A.M. Karim, D.J. Heldebrant, X. Wang, T. Peterson, Y. Wang, Aqueous phase reforming of glycerol for hydrogen production over Pt-Re supported on carbon, Appl. Catal. B Environ. 99 (2010) 206–213. https://doi.org/10.1016/j.apcatb.2010.06.021.

[78] T. Montini, M. Monai, A. Beltram, I. Romero-Ocaña, P. Fornasiero, H2 production by photocatalytic reforming of oxygenated compounds using TiO2-based materials, Mater. Sci. Semicond. Process. 42 (2016) 122–130. https://doi.org/10.1016/j.mssp.2015.06.069.

[79] T. Montini, V. Gombac, L. Sordelli, J.J. Delgado, X. Chen, G. Adami, P. Fornasiero, Nanostructured Cu/TiO2 Photocatalysts for H2 Production from Ethanol and Glycerol Aqueous Solutions., ChemCatChem. 3 (2011) 574–577. https://doi.org/10.1002/cctc.201000289.

[80] C. Minero, A. Bedini, V. Maurino, Glycerol as a probe molecule to uncover oxidation mechanism in photocatalysis, Appl. Catal. B Environ. 128 (2012) 135–143. https://doi.org/10.1016/j.apcatb.2012.02.014.

[81] E. Jolimaitre, D. Delcroix, N. Essayem, C. Pinel, M. Besson, Dihydroxyacetone conversion into lactic acid in an aqueous medium in the presence of metal salts: Influence of the ionic

thermodynamic equilibrium on the reaction performance, Catal. Sci. Technol. 8 (2018) 1349–1356. https://doi.org/10.1039/c7cy02385e.

[82] A. Takagaki, H. Goto, R. Kikuchi, S.T. Oyama, Silica-supported chromia-titania catalysts for selective formation of lactic acid from a triose in water, Appl. Catal. A. 570 (2019) 200–208. https://doi.org/10.1016/j.apcata.2018.11.018.

[83] M.A. Haider Shipar, Formation of methyl glyoxal in dihydroxyacetone and glycine Maillard reaction: A computational study, Food Chem. 98 (2006) 395–402. https://doi.org/10.1016/j.foodchem.2005.03.042.

[84] K.M.A. Santos, E.M. Albuquerque, G. Innocenti, L.E.P. Borges, C. Sievers, M.A. Fraga, The Role of Brønsted and Water-Tolerant Lewis Acid Sites in the Cascade Aqueous-Phase Reaction of Triose to Lactic Acid, ChemCatChem. (2019) 3054–3063. https://doi.org/10.1002/cctc.201900519.

[85] S. Lux, M. Siebenhofer, Catalytic conversion of dihydroxyacetone to lactic acid with Brønsted acids and multivalent metal ions, Chem. Biochem. Eng. Q. 29 (2015) 575–585. https://doi.org/10.15255/CABEQ.2014.2110.

[86] M. Hara, K. Nakajima, K. Kamata, Recent progress in the development of solid catalysts for biomass conversion into high value-added chemicals, Sci. Technol. Adv. Mater. 16 (2015) 034903(22). https://doi.org/10.1088/1468-6996/16/3/034903.

[87] R.S. Assary, L.A. Curtiss, Theoretical study of 1,2-hydride shift associated with the isomerization of glyceraldehyde to dihydroxy acetone by Lewis acid active site models, J. Phys. Chem. A. 115 (2011) 8754–8760. https://doi.org/10.1021/jp204371g.